Supplementary Information

Interface-engineered silicon nano-quill electrodes for durable extreme temperature lithium-ion batteries

Janak Basel [a, b, 1], Morteza Sabet [b, c 1 *], Peshal Karki [a, b], Mihir Parekh [a, b], Talia M. Sebastian [d], Yi Ding [d], Apparao M. Rao [a, b *]

[a] Department of Physics and Astronomy, Clemson University, Clemson, SC 29634, USA

[b] Clemson Nanomaterials Institute, Clemson University, Anderson, SC 29625, USA

[c] Department of Automotive Engineering, Clemson University, Greenville, SC 29607, USA

[d] US Army DEVCOM GVSC, Warren, MI 48397, USA

[1] Author contributed equally to this work.

* Corresponding authors: arao@clemson.edu, ssabet@clemson.edu

Number of pages: 11

Number of tables: 2

Number of figures: 4

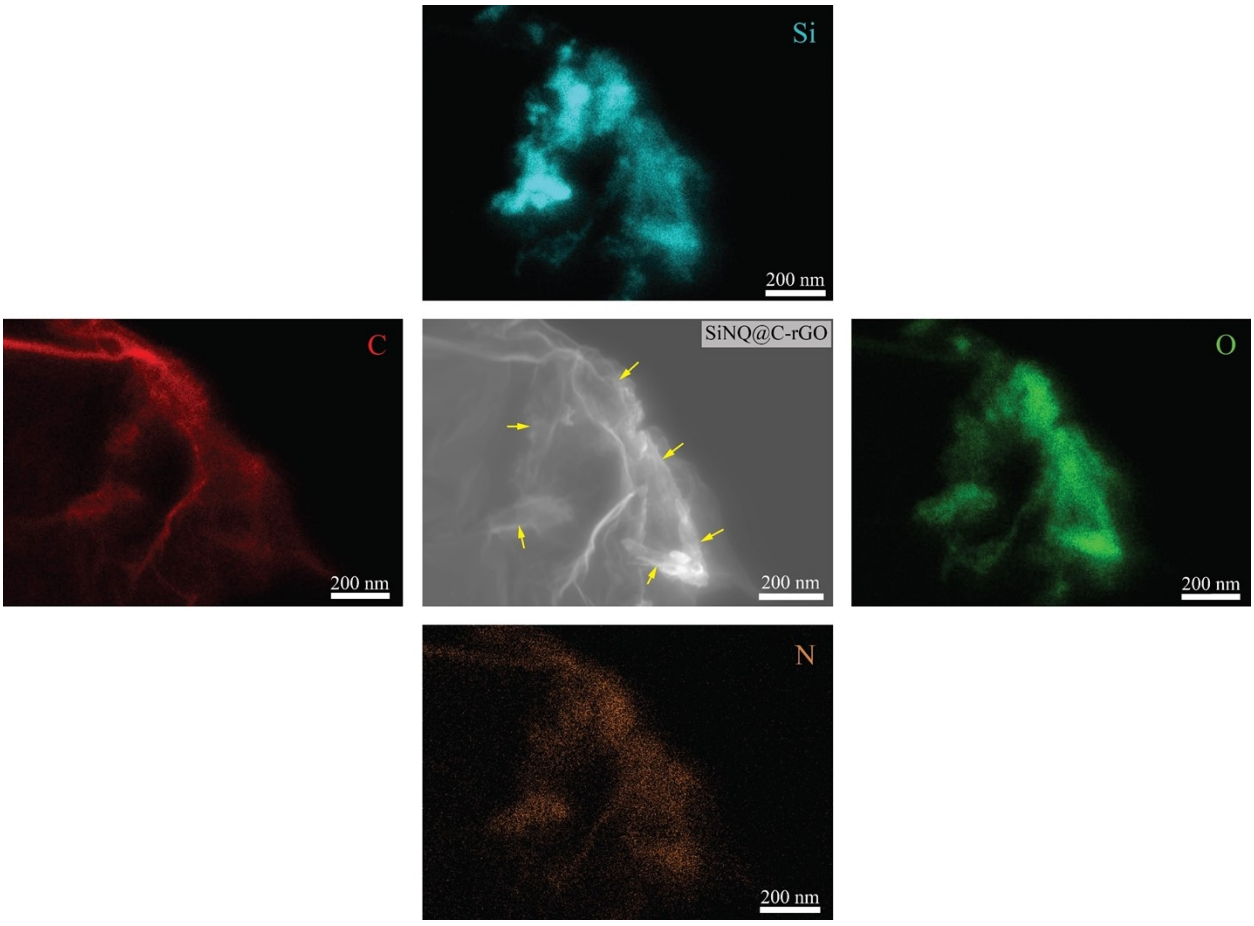

Figure S1: S-TEM image and corresponding elemental maps for several SiNQs within the SiNQ@C-rGO composite. Tubular SiNQ particles (marked by yellow arrows) are coated with an N-doped carbon shell and confined by a flexible rGO sheet.

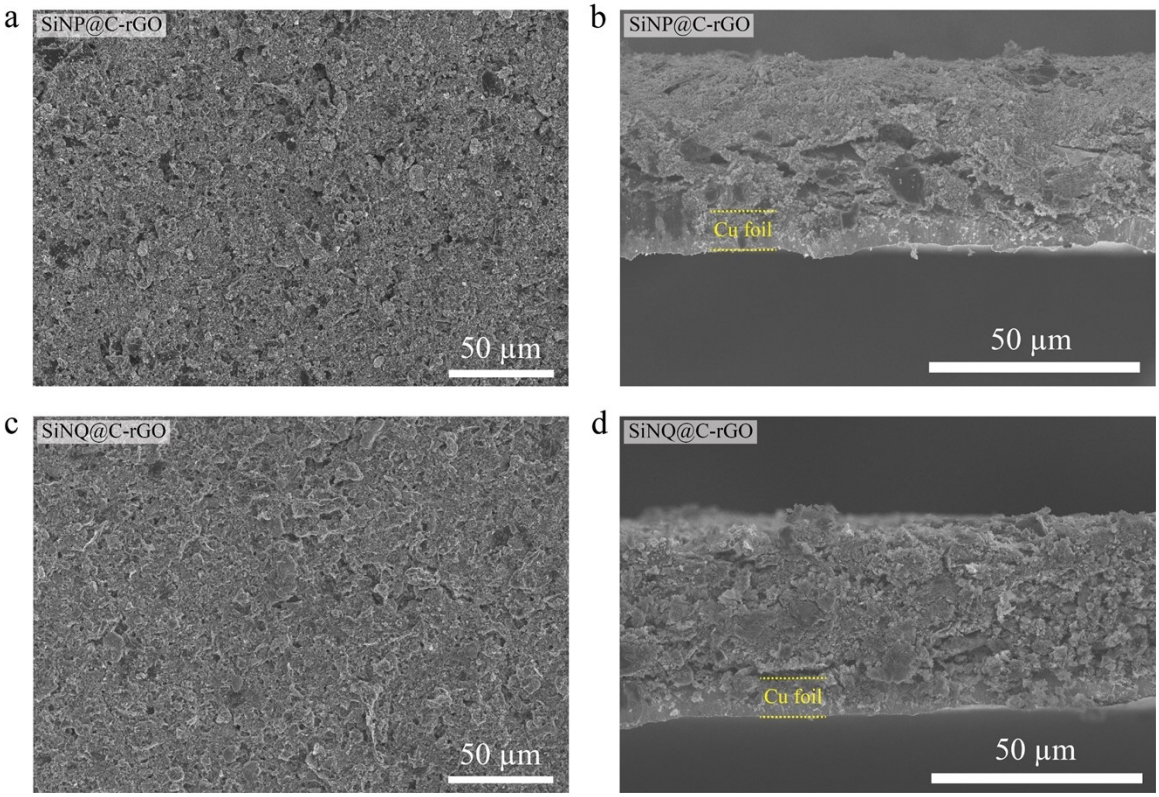

Figure S2: (a) Top-view and (b) cross-sectional view SEM images of the fabricated SiNP@C-rGO electrode; (c) Top-view and (d) cross-sectional view SEM images of the fabricated SiNQ@C-rGO electrode. The SiNP@C-rGO and SiNQ@C-rGO composite particles are uniformly distributed across the electrode coating volume.

Further insights into the cycling behavior of SiNQ@C-rGO and SiNP@C-rGO cells

The variations in charge and discharge capacity of the cells during cycling at 100 °C are presented in Figures S3a and S3b. For the SiNQ@C-rGO cell (Figure S3b), the difference between discharge and charge capacities continuously decreases up to around 67 cycles. A constantly higher capacity during electrode lithiation (discharge) than delithiation (charge) may either be a result of (a) constant Li consumption for SEI formation, since SEI formation rates are higher during lithiation than delithiation, or (b) constant trapping of Li inside the active material (in other words, not all inserted Li can be extracted). While constant trapping of Li in the active material is a possibility if Li transport within the active phase is limited due to slow diffusion, in such scenarios, it is highly unlikely that the discharge (lithiation) capacity would increase because the trapped Li would reduce the amount of active material available for lithiation during the next cycle. However, Figure S3b depicts a rise in discharge capacity from time to time, thus making reason (b) highly unlikely. Additionally, as shown in Figure S3b, when the charge and discharge capacities are nearly equal, the charge capacity rises above the discharge capacity before falling below it again in the next few cycles. This leads us to hypothesize that (i) the constantly reducing difference between charge and discharge capacities is because the SEI layer is self-passivating, and gradual SEI buildup over cycles lowers the SEI formation rate, (ii) the SEI layer ruptures after every few cycles, releasing Li previously consumed in SEI formation and leading to enhanced charge capacities, and (iii) the ruptured SEI exposes fresh surfaces that promote new SEI formation, setting the active material into a recurring cycle of SEI buildup followed by rupture. The differential capacity curves for the SiNQ@C-rGO cell corresponding to cycles 67, 68, and 69 are depicted in Figure S3c. This hypothesis is further confirmed by the presence of (a) a smooth broad peak around ~0.5–0.7 V during delithiation for cycles 67 and 68, (b) the sudden appearance of multiple broad peaks between ~0.5–1 V during the charging half-cycle of the 68th cycle (which implies the release of Li from the SEI, as Si, SiO_x, or carbon are not expected to show delithiation peaks in this voltage range), and (c) the narrowing and deepening of this peak for cycle 69, which immediately follows the SEI rupture during the charging half-cycle of the 68^{th} cycle.

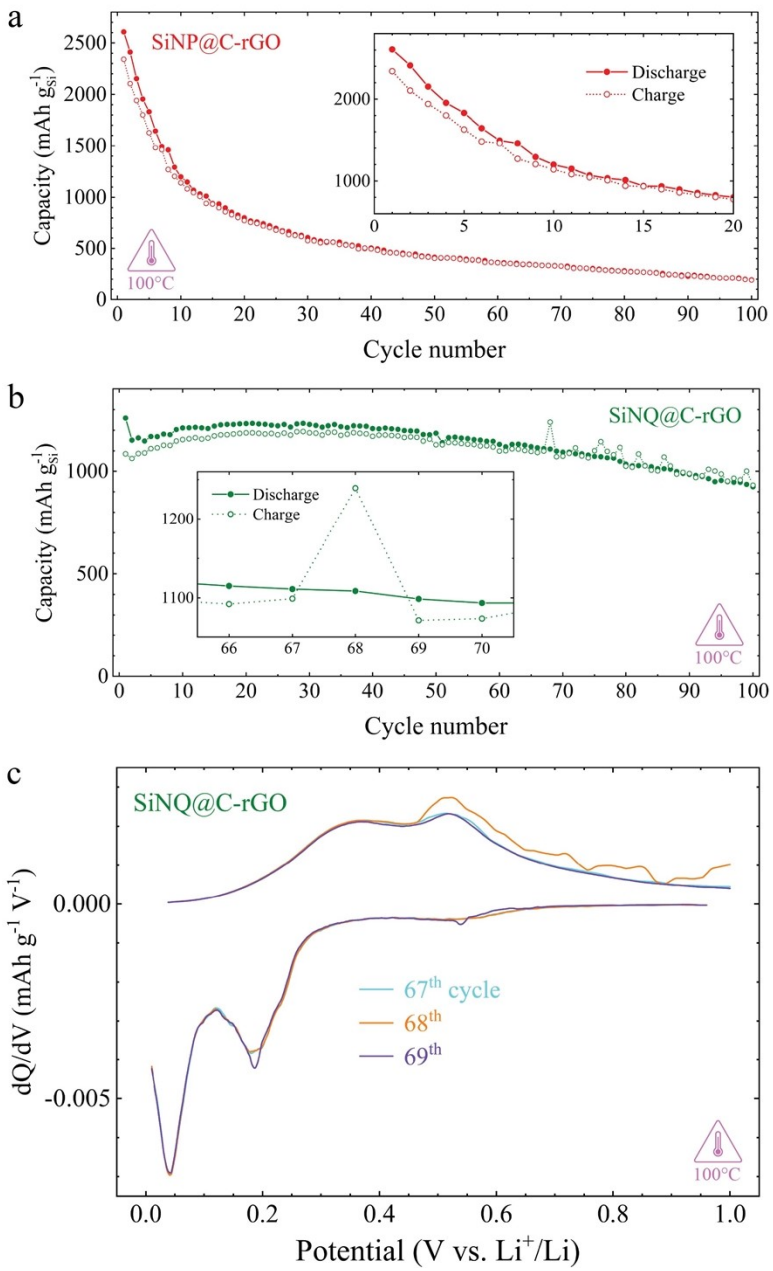

Figure S3: Charge and discharge capacities as a function of cycle number for (a) SiNP@C-rGO and (b) SiNQ@C-rGO half-cells. Insets show the magnified view of specific cycles. (c) Differential capacity curves of the SiNQ@C-rGO cell corresponding to specific cycle numbers.

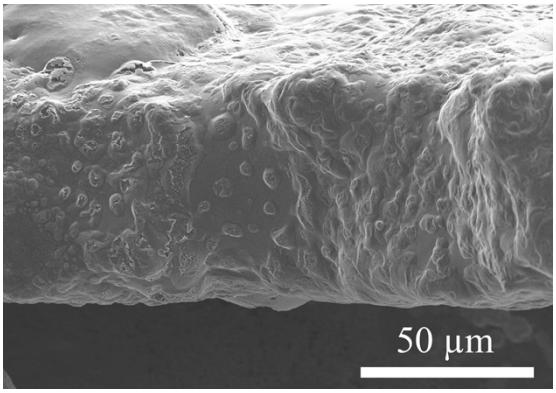

Figure S4: Cross-sectional SEM image of the SiNQ@C-rGO electrode after 100 cycles at 100 °C.

Table S1: A literature survey of the electrochemical performance of positive and negative electrodes developed for extreme batteries at or above 100 °C.

Electrode	Active material	Active loading (mg cm^{-2})	Electrolyte composition	Separator	Temperature (ºC)	Voltage (V)	Current (mA g^{-1})	1st cycle (reversible) capacity	Capacity retention (Cycle number)	Capacity loss rate (%/cycle)	Ref
Cathode	LFP	-	0.5 M LiBOB in PC	Thermosetting polyimide (PI) nano-fibers based nonwoven	120	2.5-4	124	142 mAh g^{-1}	86% (50)	0.28	1
	nano LFP (~40 nm)	-	1M LiBOB in EC	Whattman GF/d borosilicate glass fiber	100	3-3.75	~8.5	110 mAh g^{-1}	75% (170)	0.15	2
	LFP	~2	1 M LiTFSI in EMI-TFSI (IL) EMI:1-ethyl-3-methylimidazolium	polybenzimidazole (PBI) with AlN nanowires (PBI-AlN)	100	2.5-4	~510	150.5 mAh g^{-1}	98.2% (150)	0.01	3
	LFP	~2	1 M LiTFSI in EMI-TFSI (IL) EMI:1-ethyl-3-methylimidazolium	polybenzimidazole (PBI) with AlN nanowires (PBI-AlN)	100	2.5-4	~1360	~140 mAh g^{-1}	~70% (200)	0.15	3
	LFP	13	1 M LIBOB in 1/1 EC/PC + 5% VC	Al_2O_3-poly(vinylidene fluoride) nanoporous (Pyrolux™)	120	2.5-4	49.5	155 mAh g^{-1}	>90% (35)	2.57	4
	LFP	~2.85	LiFSI/$LiNO_3$/TEGDME 1/1/2.3	Celgard 2325	100	2.5-3.8	34	~165 mAh g^{-1}	89% (50)	0.22	5
	LFP/C composite	-	0.8 M LiTFSI in Pip-TFSI	quartz membrane	120	3-4.5	~34	140 mAh g^{-1}	80% (100)	0.2	6
	LFP	10.2	0.5 M LiBF4/0.5M LiDFOB in EC/PC/DEC (0.2:1.8:0.5 v/v)	Celgard 2400	120	2.0–4.0	~85 ~170	159 mAh g^{-1} 153.5 mAh g^{-1}	97% (57) 98.6% (120)	0.05 0.01	7
	LFP	~5	0.5 M LiDFOB in (glycerol triacetate)GTA/FEC = 5:2 (v/v)	Celgard 3401 surfactant-coated	100	3-4.3	~34	~160 mAh g^{-1}	95.6% (100)	0.04	8
	NCM523	~5	0.5 M LiDFOB in (glycerol triacetate)GTA/FEC = 5:2 (v/v)	Celgard 3401 surfactant-coated	100	3-4.3	~170	~170 mAh g^{-1}	65.6% (100)	0.34	8
	NMC532	-	0.5 mol/L LiTFSI in Ph_{1444}TFSI with 0.5 w/v % LiDFOB	Celgard PP2075	100	2.8-4.0	30	~138 mAh g^{-1}	90% (100)	0.1	9
	NCM811	-	1 M LiTFSI/triethyl phosphate(TEP) with 2% FEC	-	100	2.8-4.2	~200	~145 mAh g^{-1}	~75% (50)	0.5	10
	Graphite	5.5	1 M LIBOB in 1/1 EC/PC + 5% VC	Al_2O_3-poly(vinylidene fluoride) nanoporous (Pyrolux™)	120	0.01-1	109	340 mAh g^{-1} ~1.87 mAh cm^{-2}	>90% (100)	0.1	4
	Graphite	2-3	4 M LiFSA in DMC	Polyethylene	100	0.01-1.8	744	~372 mAh g^{-1} ~0.93 mAh cm^{-2}	76% (500)	0.05	11
	LTO	-	clay/PPMI-(1 M) LiTFSI composite, PPMI:1-Methyl-1-propylpiperidinium	-	120	1.0-2.0	50	65 mAh g^{-1}	~88% (120)	0.1	12
	LTO	2.92	0.8 M LiTFSI and 0.2 M LiODFB in Adiponitrile(ADN)/EC (v/v 1 : 1)	glass fibre	100	1.0-3.0	~875	~140 mAh g^{-1} ~0.41 mAh cm^{-2}	99.93% (1000)	0.00007	13

	LTO	2.92	0.8 M LiTFSI and 0.2 M LiODFB in Adiponitrile(ADN)/EC (v/v 1 : 1)	glass fibre	120	1.0-3.0	~875	~174 mAh g^{-1} ~0.51 mAh cm^{-2}	87.94% (1000)	0.01	13
	LTO	5-7	h-BN composite (Mix of boron nitride powder and a 1 M solution of LiTFSI in 1-methyl-1-propylpiperidinium bis(trifl uoromethylsulfonyl)imide, in a 1:2 w/w ratio)	-	120	1.0-3.0	~22	158 mAh g^{-1} ~0.95 mAh cm^{-2}	~99% (50)	0.02	14
	LTO	5-7	h-BN composite (Mix of boron nitride powder and a 1 M solution of LiTFSI in 1-methyl-1-propylpiperidinium bis(trifl uoromethylsulfonyl)imide, in a 1:2 w/w ratio)	-	120	1.0-3.0	~87.5	~160 mAh g^{-1} ~0.96 mAh cm^{-2}	~94% (45)	0.13	14
	3D Si (Si sputtered on 3D Ni current collector)	~0.21	0.8 M LiTFSI in Pip-TFSI (Pip:1-methyl-1-propylpiperidinum)	quartz membrane	100	0.05-1.5	840	~0.41 mAh cm^{-2}	~83% (30)	0.34	15
		~0.23	0.8 M LiTFSI in Pip-TFSI + 20% PC (v/v)		100		8400	~0.21 mAh cm^{-2}	~86% (60)	0.23	15
		-	0.8 M LiTFSI in Pip-TFSI		120		840	~0.49 mAh cm^{-2}	~89% (200)	0.06	6
		-	0.8 M LiTFSI in Pip-TFSI		150		840	~0.44 mAh cm^{-2}	~70% (200)	0.15	6
	SiNQ@C-rGO	0.8-0.9	0.8 M LiTFSI in Pip-TFSI	Celgard 2325	100	0.01-1	420	1260 mAh g^{-1} 1.13 mAh cm^{-2}	~73% (100)	0.27	**This work**

Table S2: Gas physisorption results for pristine SiNP and SiNQ powders and their corresponding composite materials.

Sample	Specific surface area ($m^2 g^{-1}$)	Total pore volume ($cm^3 g^{-1}$)
SiNP	56.15	0.12
SiNP@C-rGO	22.98	0.05
SiNQ	399.46	0.64
SiNQ@C-rGO	487.95	0.88

References

(1) Jiang, W.; Liu, Z.; Kong, Q.; Yao, J.; Zhang, C.; Han, P.; Cui, G. A High Temperature Operating Nanofibrous Polyimide Separator in Li-Ion Battery. *Solid State Ion.* **2013**, *232*, 44–48. https://doi.org/10.1016/j.ssi.2012.11.010.

(2) Mestre-Aizpurua, F.; Hamelet, S.; Masquelier, C.; Palacín, M. R. High Temperature Electrochemical Performance of Nanosized LiFePO4. *J. Power Sources* **2010**, *195* (19), 6897–6901. https://doi.org/10.1016/j.jpowsour.2010.03.097.

(3) Guo, Y.; Feng, B.; Wang, Y.; Zhao, J.; Zhou, C.; Wang, X.; Yang, L.; Jin, Z.; Hu, Z.; Wu, Q. A Thermally Managed Separator for Lithium Metal Batteries Operating Safely above 100 °C. *Nano Energy* **2025**, *133*. https://doi.org/10.1016/j.nanoen.2024.110472.

(4) Kohlmeyer, R. R.; Horrocks, G. A.; Blake, A. J.; Yu, Z.; Maruyama, B.; Huang, H.; Durstock, M. F. Pushing the Thermal Limits of Li-Ion Batteries. *Nano Energy* **2019**, *64*. https://doi.org/10.1016/j.nanoen.2019.103927.

(5) Chen, T.; Jin, Z.; Liu, Y.; Zhang, X.; Wu, H.; Li, M.; Feng, W. W.; Zhang, Q.; Wang, C. Stable High-Temperature Lithium-Metal Batteries Enabled by Strong Multiple Ion–Dipole Interactions. *Angewandte Chemie - International Edition* **2022**, *61* (35). https://doi.org/10.1002/anie.202207645.

(6) Ababtain, K. A. *Design And Optimization Of Lithium Ion Battery For High Temperature Applications*; 2016. https://digitalcommons.wayne.edu/oa_dissertations/1613.

(7) Xu, C.; Chen, C.; Xia, W.; Zhou, H.; Zhang, S.; Wu, M. Dual Anion-Regulated Solvation Structure Enables LiFePO4 Batteries with Ultra-Wide Temperature Operation (−40–130 °C). *Chemical Engineering Journal* **2025**, *522*. https://doi.org/10.1016/j.cej.2025.168146.

(8) Wu, X.; Liu, T.; Lee, Y. G.; Whitacre, J. F. Glycerol Triacetate-Based Flame Retardant High-Temperature Electrolyte for the Lithium-Ion Battery. *ACS Appl. Mater. Interfaces* **2024**, *16* (19), 24590–24600. https://doi.org/10.1021/acsami.4c02323.

(9) Nagarajan, S.; Hwang, S.; Jaye, C.; Weiland, C.; Meira, D. M.; Balasubramanian, M.; Arava, L. M. R. Investigation of Electrode-Electrolyte Interfaces to Enable Non-Flammable Li-Ion Batteries Operating up to 125°C with Liquid Electrolyte. *Cell Rep. Phys. Sci.* **2025**, *6* (5). https://doi.org/10.1016/j.xcrp.2025.102597.

(10) Jiang, L.; Liang, C.; Li, H.; Wang, Q.; Sun, J. Safer Triethyl-Phosphate-Based Electrolyte Enables Nonflammable and High-Temperature Endurance for a Lithium Ion Battery. *ACS Appl. Energy Mater.* **2020**, *3* (2), 1719–1729. https://doi.org/10.1021/acsaem.9b02188.

(11) Wang, J.; Zheng, Q.; Fang, M.; Ko, S.; Yamada, Y.; Yamada, A. Concentrated Electrolytes Widen the Operating Temperature Range of Lithium-Ion Batteries. *Advanced Science* **2021**, *8* (18). https://doi.org/10.1002/advs.202101646.

(12) Kalaga, K.; Rodrigues, M. T. F.; Gullapalli, H.; Babu, G.; Arava, L. M. R.; Ajayan, P. M. Quasi-Solid Electrolytes for High Temperature Lithium Ion Batteries. *ACS Appl. Mater. Interfaces* **2015**, *7* (46), 25777–25783. https://doi.org/10.1021/acsami.5b07636.

(13) Zheng, T.; Xiong, J.; Zhu, B.; Shi, X.; Cheng, Y. J.; Zhao, H.; Xia, Y. From −20 °C to 150 °C: A Lithium Secondary Battery with a Wide Temperature Window Obtained via Manipulated Competitive Decomposition in Electrolyte Solution. *J. Mater. Chem. A Mater.* **2021**, *9* (14), 9307–9318. https://doi.org/10.1039/d1ta00895a.

(14) Rodrigues, M. T. F.; Kalaga, K.; Gullapalli, H.; Babu, G.; Reddy, A. L. M.; Ajayan, P. M. Hexagonal Boron Nitride-Based Electrolyte Composite for Li-Ion Battery Operation from Room Temperature to 150 °C. *Adv. Energy Mater.* **2016**, *6* (12). https://doi.org/10.1002/aenm.201600218.

(15) Ababtain, K.; Babu, G.; Lin, X.; Rodrigues, M. T. F.; Gullapalli, H.; Ajayan, P. M.; Grinstaff, M. W.; Arava, L. M. R. Ionic Liquid-Organic Carbonate Electrolyte Blends to Stabilize Silicon Electrodes for Extending Lithium Ion Battery Operability to 100 °c. *ACS Appl. Mater. Interfaces* **2016**, *8* (24), 15242–15249. https://doi.org/10.1021/acsami.6b02620.